Multi-wavelength follow-up of FRB 180309

KSHITIJ AGGARWAL , 1,2 SARAH BURKE-SPOLAOR , 1,2 NICOLAS TEJOS , 3 GIULIANO PIGNATA , 4,5 J. XAVIER PROCHASKA , VIKRAM RAVI , 5 JANE F. KACZMAREK , 9 AND STEFAN OSŁOWSKI , 11

West Virginia University, Department of Physics and Astronomy, P. O. Box 6315, Morgantown, WV, USA
 Center for Gravitational Waves and Cosmology, West Virginia University, Chestnut Ridge Research Building, Morgantown, WV, USA
 Instituto de Física, Pontificia Universidad Católica de Valparaíso, Casilla 4059, Valparaíso, Chile
 Departamento de Ciencias Fisicas, Universidad Andres Bello, Avda. Republica 252, Santiago, Chile
 Millennium Institute of Astrophysics (MAS), Nuncio Monsenor Sotero Sanz 100, Providencia, Santiago, Chile
 University of California Observatories-Lick Observatory, University of California, 1156 High Street, Santa Cruz, CA95064, USA
 Kavli Institute for the Physics and Mathematics of the Universe (WIP), 5-1-5 Kashiwanoha, Kashiwa, 277-8583, Japan
 Cahill Center for Astrophysics, California Institute of Technology, Pasadena, CA 91125, USA
 CSIRO Astronomy and Space Science, Australia Telescope National Facility, Box 76, Epping, NSW 1710, Australia
 Gravitational Wave Data Centre, Swinburne University of Technology, P.O. Box 218, Hawthorn, VIC 3122, Australia
 Centre for Astrophysics and Supercomputing, Swinburne University of Technology, P.O. Box 218, Hawthorn, VIC 3122, Australia

(Received -; Revised -; Accepted -) Submitted to ApJ

ABSTRACT

We report on the results of multi-wavelength follow-up observations with Gemini, VLA, and ATCA, to search for a host galaxy and any persistent radio emission associated with FRB 180309. This FRB is among the most luminous FRB detections to date, with a luminosity of $> 8.7 \times 10^{32}$ erg Hz⁻¹ at the dispersion-based redshift upper limit of 0.32. We used the high-significance detection of FRB 180309 with the Parkes Telescope and a beam model of the Parkes Multibeam Receiver to improve the localization of the FRB to a region spanning approximately $\sim 2' \times 2'$. We aimed to seek bright galaxies within this region to determine the strongest candidates as the originator of this highly luminous FRB. We identified optical sources within the localization region above our r-band magnitude limit of 24.27, fourteen of which have photometric redshifts whose fitted mean is consistent with the redshift upper limit (z < 0.32) of our FRB. Two of these galaxies are coincident with marginally detected "persistent" radio sources of flux density $24.3 \,\mu\text{Jy} \,\text{beam}^{-1}$ and $22.1 \,\mu\text{Jy} \,\text{beam}^{-1}$ respectively. Our redshift-dependent limit on the luminosity of any associated persistent radio source is comparable to the luminosity limits for other localized FRBs. We analyze several properties of the candidate hosts we identified, including chance association probability, redshift, and presence of radio emission, however it remains possible that any of these galaxies could be the host of this FRB. Follow-up spectroscopy on these objects to explore their $H\alpha$ emission and ionization contents, as well as to obtain more precisely measured redshifts, may be able to isolate a single host for this luminous FRB.

Keywords: Radio transient sources(2008) — Radio continuum emission(1340) — Radio interferometry(1346) — Optical observation(1169) — Optical identification(1167) — Radio galaxies(1343) — Extragalactic radio sources(508) — Radio bursts(1339) — Very Large Array(1766)

1. INTRODUCTION

Corresponding author: Kshitij Aggarwal ka0064@mix.wvu.edu

Fast Radio Bursts (FRBs) are bright, millisecondduration radio transients of unknown origin and are characterized by dispersion measures (DM) that are much higher than the Milky Way's contribution in a given direction (Lorimer et al. 2007). Hundreds of such

bursts have been seen so far, most of which have been one-off events, while some have been seen to repeat (Petroff et al. 2016).

In only the past three years, a number of FRBs have been localized using the Australian Square Kilometre Array Pathfinder (ASKAP), Deep Synoptic Array (DSA), the European VLBI Network (EVN), and the REALFAST/Very Large Array (VLA) experiment (Bannister et al. 2019; Ravi et al. 2019; Prochaska et al. 2019; Marcote et al. 2020; Law et al. 2020; Macquart et al. 2020). The repetitions of the first known repeating FRB, FRB 121102, led to its sub-arcsecond localization (Chatterjee et al. 2017). It was further associated with a lowmetallicity faint dwarf galaxy at z = 0.19 (Tendulkar et al. 2017). It is also coincident with a highly compact (projected size < 0.7 pc), persistent (non-bursty) radio source of flux density $S_{2 \text{ GHz}} \sim 150 \mu \text{Jy}$, which has a distinct spectrum that is relatively flat out to around 8 GHz, and declines above that cutoff (Chatterjee et al. 2017; Marcote et al. 2017). While the same report indicated that chance coincidence of this emission's colocation with the FRB is exceedingly small $(P < 10^{-5})$, it remains possible that the emission colocated with FRB 121102 is simply a red herring, and not specifically caused by or related to the FRB.

The properties of the subsequently localized bursts and their hosts are markedly different from that of FRB 121102, ranging from massive elliptical galaxies to luminous spiral galaxies (Bannister et al. 2019; Ravi et al. 2019; Prochaska et al. 2019; Bhandari et al. 2020; Marcote et al. 2020). Only one other repeating FRB (FRB 180916.J0158+65) has been localized (Marcote et al. 2020) to a star-forming region in a massive spiral galaxy. Similar to FRB 121102, FRB 180916.J0158+65 is offset from this knot of star forming region (Bassa et al. 2017; Tendulkar et al. 2021). No persistent radio emission has been detected in any of these other localized FRBs. It is to be noted that upper limits on persistent radio emission for some of these FRBs are a few orders of magnitude less than the persistent emission detected for FRB 121102 (Marcote et al. 2020; Macquart et al. 2020). Thus, it appears that FRBs may originate from a variety of host galaxies and environments (Heintz et al. 2020). Recently, luminous radio bursts have been detected from a Galactic magnetar SGR 1935+2154, providing evidence that some FRBs may be emitted by magnetars at cosmological distances and originate from Milky Way like galaxies (Bochenek et al. 2020; CHIME/FRB Collaboration et al. 2020; Kirsten et al. 2020).

Sub-arcsecond localization is generally essential for conclusive identification of an FRB with a counterpart or host galaxy (Eftekhari & Berger 2017; Bloom et al. 2002). This is crucial to understanding the progenitors of FRBs and their host environments. But subarcsecond localization is only possible with interferometers with realtively large baselines like VLA, ASKAP and EVN. With single-dish telescopes, the localization is limited by the beam size, which is usually several arcminutes. Multibeam receivers, like the ones at Parkes (Staveley-Smith et al. 1996), and Focal L-band Array for the Green Bank Telescope (Rajwade et al. 2018), can improve localization if a signal is bright enough to appear in multiple beams, allowing one to fit the relative signal strength in each beam to the side-lobe pattern of the multiple beams. This technique has been used to some success for past bursts; for instance, Ravi (2019) localized FRB 010724 (detected in 3 beams with a 1-bit system) to around 50 arcmin² with no frequency information or calibration. With an improved 8-bit observing system, Ravi et al. (2016) was able to localize FRB 150807 with two beams to around 9 arcmin².

Osłowski et al. (2019) reported the discovery of four FRBs found with the commensal FRB search system at Parkes Telescope. These FRBs were detected during the Parkes Pulsar Timing Array observations of millisecond pulsars. Of these four, FRB 180309 was the strongest FRB vet detected, with a fluence (F > 83.5 Jy ms) that was so bright that it saturated the central beam of the Parkes Telescope Multibeam Receiver (Staveley-Smith et al. 1996). It was detected at a DM of 263.42 pc cm $^{-3}$ and was narrowest of those 4 FRBs with a width of 0.475 ms. Osłowski et al. (2019) estimated its redshift to be z < 0.19 and calculated the linear and circular polarization fractions to be $L_{\rm f} = 0.4556 \pm 0.0006$ and $V_{\rm f} = 0.2433 \pm 0.0005$. They also placed an upper limit of 150 rad m^{-2} on the modulus of the rotation measure of this FRB. More importantly, it was also detected in six other beams, with a flux fall-off that matches that expected from side-lobe detection from those beams (i.e. this signal was localized on the sky roughly boresight to the pointing position, and is not like the terrestrial peryton signals reported by Burke-Spolaor et al. 2011). Given the seven-beam detection of FRB 180309 and fully calibrated spectra, it is possible to greatly improve the standard $14' \times 14'$ localization typically provided by Parkes.

In this paper, we summarize the process for improving the localization of this FRB to approximately $2' \times 2'$. We performed multi-frequency follow-up observations of this error region to search for optical host galaxy candidates and any candidates for persistent radio sources related to the FRB within its DM-based redshift upper limit. In $\S 2$ we describe radio and optical follow-up ob-

servations. In $\S 3$ we re-examine the likely redshift range of the FRB based on DM-z relationships that have been updated since the publication of Osłowski et al. (2019). We describe the procedure of fitting the beam pattern to obtain a more precise localization in $\S 4$. $\S 5$ presents the results of our observations, and we discuss the implications of our analysis and results in $\S 6$.

2. OBSERVATIONS

2.1. VLA Data

We performed observations with the VLA on 2018 March 23, 14 days after the detection of the FRB. The VLA was in A-configuration, and the observing project code was VLA/18A-462. The central observing frequency was 2999 MHz, with a total bandwidth of 2048 MHz divided into 1024, 2 MHz-wide contiguous frequency channels, and two polarizations. Our pointing center was directed at position R.A.= 21^h24^m19^s.15, Decl.=-33°56′10″ (J2000), which is the pointing center reported by Osłowski et al. (2019). We used a 2s sampling interval. The standard primary calibrator 3C48 was used for flux density and bandpass calibration, and source J2109-4110 was used as a phase calibrator. We obtained a total on-source time of 1.15 hr.

We calibrated the data using the standard VLA calibration pipeline, followed by manual flagging and imaging with the CASA software package¹. We interactively deconvolved the images using the TCLEAN task, with natural weighting to maximize image sensitivity. We obtained an RMS of $5.7\,\mu\mathrm{Jy\,beam^{-1}}$ in the central regions of our final image. The synthesized beam major and minor axes were 1.86'' and 0.67'' respectively, and the beam position angle was -8.6° .

2.2. Optical Imaging Data

We observed the field towards FRB 180309 using the Gemini Multi-Object Spectrograph (GMOS; Hook et al. 2004; Gimeno et al. 2016) on Gemini-South. We obtained a set of $1\times300\,\mathrm{s}$ images in the i and z bands on UT 2018 March 28 (19 days after the FRB) and a set of $3\times300\,\mathrm{s}$ and $4\times300\,\mathrm{s}$ images in the g and r-bands, respectively, on UT 2018 April 19 (41 days after the FRB). We reduced and co-added these images with Pyrafe using standard procedures. In the z band, before combining, we remove the fringe pattern using a fringe map provided by the Gemini Observatory. The astrometric solution for the images was computed using 16 stars identified in our r-band image, which were also present

in the GAIA DR2 catalog. Comparing the positions of these stars, we obtained a root mean square uncertainty of 0.038" and 0.041" in R.A. and Decl. respectively. We performed optical photometry for the sources within the uncertainty region to the FRB 180309 (see Section 4 for details of localization region) using SExtractor package (Bertin & Arnouts 1996) with the r-band image, which was the most sensitive among all the images, adopted as the reference for source detection. We measured the galaxy magnitudes in all bands using flux_auto with an aperture of 2.5 times the Kron radius, which includes >96\% of the total flux of the galaxy (Kron 1980). We corrected these magnitudes to the total flux by measuring the growth curve of isolated stars out to a radius of 10". As visible in Table 3, the faintest detected galaxy has a r-band magnitude of 24.27, which can provide an estimation of the achieved completeness.

We estimated photometric redshifts for these galaxies using the EAZY software (Brammer et al. 2008) and report the 95% c.l. values; the Galactic extinction is low in the field direction (Schlafly & Finkbeiner 2011), and thus we did not correct it.

We performed an astrometric comparison of the VLA radio and optical images to check and correct any systematic offset between the two. We identified three sources lying outside the localization region of the FRB, which were clearly detected in both the images. These sources were above a significance of 7σ in radio and above the optical magnitude limit. Details of these sources, along with their respective offsets, are given in Table 1. We calculated an average offset of 0.132" in RA and 1.7826" in DEC between the two images. This offset was corrected for by shifting the radio image. We recognized that the offset in declination was far greater than the phase-referencing astrometric standard typically reached with the VLA; we determined (in private communication with L. Sjouwerman of NRAO) that this offset was likely due to a combination of the relatively large offset between phase calibrator and target (\sim 8 degrees) and the near-horizon observation that the low declination required of the VLA.

2.3. ATCA Data

The brightness of FRB 180309 led Osłowski et al. (2019) to search for the signature of H I absorption in the spectrum of this burst. They reported the "most prominent" absorption feature (2.8 σ ; private correspondence) at 1386 MHz, implying a source redshift of z=0.025. The redshift of this feature is consistent with the redshift upper limit for this FRB (see Section 3). Therefore, we collected data with the Australia Telescope Compact

https://casa.nrao.edu/

https://www.gemini.edu/sciops/data-and-results/ processing-software

Sr. No	Radio	Optical	Offset (")			
	RA	DEC	RA	DEC	RA	DEC
1	$21:24:7.0598\pm0.0029$	$-33:57:28.5982 \pm 0.1876$	21:24:07.046	-33:57:30.58	0.207	1.9818
2	$21:24:11.8076\pm0.0038$	$-33:55:34.2159 \pm 0.1020$	21:24:11.802	-33:55:35.80	0.084	1.5841
3	$21:24:20.418 \pm 0.016$	$-33:54:26.528 \pm 0.193$	21:24:20.411	-33:54:28.31	0.105	1.782

Table 1. Astrometric Comparison

Array (ATCA) to search for H I signatures of host galaxies.

We took the data on 2018 July 19, 20, and 21 (132-134 days after the FRB) with the telescope in the hybrid 75 m array and recorded in both continuum and high-frequency resolution "zoom" modes. Continuum data has a center frequency of 2100 MHz with 2048, 1-MHz channels. We recorded a "zoom" band, centered on 1386 MHz with a velocity resolution of 0.11 km s $^{-1}$ and spanning the velocity range 1189.4 km s $^{-1}$.

The telescope was pointed at R.A.= $21^{\rm h}24^{\rm m}20^{\rm s}.27$, Decl.= $-33^{\circ}56'35''.10$ (J2000) and R.A.= $21^{\rm h}24^{\rm m}16^{\rm s}.65$, Decl.= $-33^{\circ}55'57''.20$ (J2000), which corresponds to the positions of the two optically-defined galaxies, m402-023014 and m402-023436 (Ungruhe et al. 2003). We did not know the redshifts of the optically identified galaxies within the field of view. Therefore, we could not point to the anticipated H I locations. As these pointings are within the same ATCA primary beam, we treat the pointings as a mosaic and combine the datasets with a total on-source time of 7.25 hours. We used standard calibrator PKS 1934–638 for bandpass and absolute flux calibration. Observations of PKS 2149–306 were taken every 40 minutes for phase and gain calibration.

We reduced the data using the MIRIAD (Sault et al. 1995) software package using standard routines. We mainly used the automated task PGFLAG for flagging of the data, with minor manual flagging using tasks BLFLAG and UVFLAG. As the two pointing centers were within half the width of the primary beam, we mosaiced the two pointings together and made a naturally-weighted total intensity map using the entire $2\,\mathrm{GHz}$ continuum bandwidth with a synthesized beam of $20\times15''$ and an RMS of $0.1\,\mathrm{mJy}$ beam⁻¹. We made the images using the compact antennas only, and excluded antenna 6 as it is located 6 km from the main array.

3. THE DM-BASED REDSHIFT OF FRB 180309

The observed DM_{FRB} for FRB 180309 as quoted by Osłowski et al. (2019) is $263.42 \pm 0.01 \,\mathrm{pc}\,\mathrm{cm}^{-3}$. We use the "FRBS" library (Prochaska et al. 2019) presented first in Prochaska & Zheng (2019) to determine local

contributions to this observed DM based on its position: those from the Milky Way's interstellar medium (DM_{MW}) and from our galaxy's halo (DM_{Halo}). We estimated DM_{MW} using two electron density models of the Galaxy: NE2001 (Cordes & Lazio 2002) and YMW16 (Yao et al. 2017). For this analysis, we also assume a conservatively small host-galaxy DM contribution of DM_{host} = $50 \, \mathrm{pc} \, \mathrm{cm}^{-3}$, which serves to account for a fairly standard contribution from a host galaxy's ISM and halo (Prochaska & Zheng 2019). This value of DM_{host} is also consistent with the empirically derived 95% confidence interval on DM_{host} obtained by Macquart et al. (2020).³

We then used the dispersion measure of FRB 180309 to estimate the likely redshift of an FRB host galaxy by subtracting the various DM contributions listed above. These estimates imply a likely range on the DM contribution from intergalactic medium (DM $_{\rm cosmic}$) to be 104–120 pc cm $^{-3}$ (see Table 2). These numbers may, of course decrease if the host DM contribution is significantly larger than what we have assumed.

From the $\mathrm{DM_{cosmic}}$ value above, we may estimate a firm upper limit to the FRB redshift and also a best estimate. For the latter, we adopt the mean Macquart relation⁴ with the cosmological parameters from (Planck Collaboration et al. 2016). This yields z=0.13. For the upper limit, we adopt the probability distribution function for $\mathrm{DM_{cosmic}}$ from Macquart et al. (2020) and assume a uniform prior in redshift to assess P(z|DM) as depicted in Figure 1. From our upper limit to $\mathrm{DM_{cosmic}}$ we set a conservative upper limit z<0.32. Wherever necessary, we use the above two redshift values to estimate the luminosities of relevant sources. It is possible that the FRB (and its host galaxy) is much closer than the DM-based redshift limit derived above, with a large

³ Note that Macquart et al. determined a galaxy-rest-frame average host DM_{rest} of $100 \,\mathrm{pc}\,\mathrm{cm}^{-3}$. However, this value is closer to our estimate here when considering the contribution to the observed DM will scale by $DM_{rest}/(1+z)$.

⁴ https://github.com/FRBs/FRB

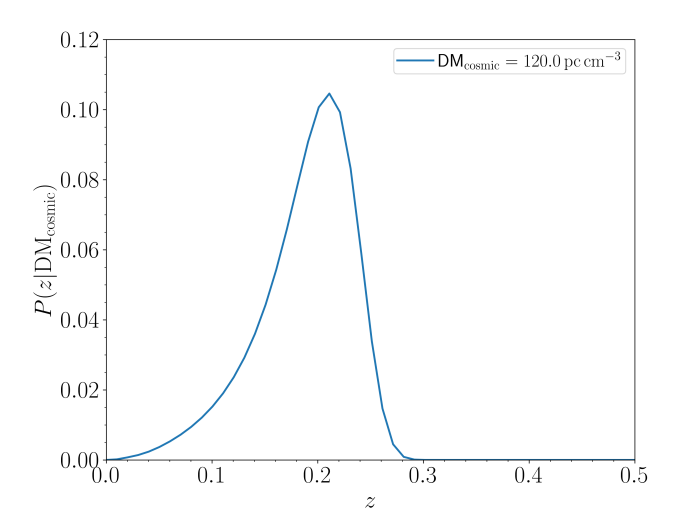


Figure 1. Probability density function $P(z|\mathrm{DM_{cosmic}})$ for $\mathrm{DM_{cosmic}} = 120\mathrm{pc}\,\mathrm{cm}^{-3}$.

Table 2. Estimate of DM_{cosmic} of FRB 180309

DM part	NE2001	YMW16		
$\overline{\mathrm{DM}_{\mathrm{FRB}}}$	263	263		
$\mathrm{DM}_{\mathrm{MW}}$	46	30		
$\mathrm{DM}_{\mathrm{Halo}}$	63	63		
$\mathrm{DM}_{\mathrm{host}}$	50	50		
$\mathrm{DM}_{\mathrm{cosmic}}$	104	120		

fraction of the dispersion measure being contributed by plasma local to the FRB.

4. THE LOCALIZATION OF FRB 180309

If we know the side-lobe structure of the Multibeam Receiver, we can use information about the beamdependent signal to noise (S/N) of a detected source to localize an FRB to a region smaller than the oft-quoted half-power beamwidth of the telescope (for Parkes at our frequency, this leads to a typical localization region of approximately 150 arcmin²). To improve the localization of FRB 180309 we performed a procedure similar to that of Ravi et al. (2016), in which the high-significance detection of FRB 150807 in multiple beams allowed us to constrain its position to a 9 arcmin² region. FRB 180309 was detected in 7 of 13 beams in the Parkes multi-beam receiver. It was saturated in beam 1, supplying only a lower limit to the actual intensity. Treating beam 1 as a lower limit, we followed the procedure as described in Ravi et al. (2016). The resulting position following

their prescription allowed localization of FRB 180309 to approximately $\sim 2' \times 2'$, as shown in Figure 2.

5. RESULTS

5.1. Objects within Localization Region

We display our radio and optical imaging of the full localization error region in Figure 2. There were no prominent ($\geq 5\sigma$) detections in the VLA radio data within or near the localization error region.

Above an r-band magnitude limit of 24.27, 20 galaxies were detected in the Gemini GMOS data within the error region. Basic measurements for these galaxies are provided in Table 3. Out of these 20 sources, 14 sources have redshift limits consistent with the range of redshifts we estimated for FRB 180309 in §3. The last column in Table 3 gives the association probability of the optical galaxy detections, as discussed later in Section 6.1.

We did not detect any steady nor transient radio source within the localization error region, down to a 5σ limit of 150μ Jy beam⁻¹, in our three-epoch ATCA data. There was no detection of H I counterparts within the localization region, at the implied redshift of the spectral feature reported by Osłowski et al. (2019).

5.2. Coincident Radio/Optical Detections

The brightest radio feature within the localization error region had a S/N of only 4.3 in our VLA imaging (corresponding to a peak flux of approximately $24.3\,\mu\mathrm{Jy\,beam^{-1}}$). Thus, while we did not detect any prominent radio sources in this field, there were two marginal radio detections (the S/N = 4.3 event and one at S/N = 3.9) that were coincident with our optical galaxy identifications; these fluxes are reported in Table 3 for sources 1 and 5. An enlarged region showing these targets is displayed in Fig 3; it is clear from this figure that while these may be genuine detections, residual low-level side-lobe features in the image may be artificially boosting the flux at these locations. These detections are discussed further in Section 6.2.

5.3. Serendipitous Detection of a Winged Field Object

In our imaged field, but far from the localization region of FRB 180309, we detected a complex radio source (hereafter referred to as J2124-3358). We show this object in Fig 4. A compact optical galaxy is co-located at the nexus of the complex structures and is presumably the host. The position of the central optical source in the Gemini r-band image is J2000 R.A.= $21^{\rm h}24^{\rm m}6^{\rm s}.171(2)$, Decl.= $-33^{\circ}58'8''.3(2)$. As this presumed host was at the edge of the optical image, the magnitudes in different optical bands were not reliable enough to determine its photometric redshift. J2124-3358 is very similar in complexity to the X-, S-, and Z-shaped sources

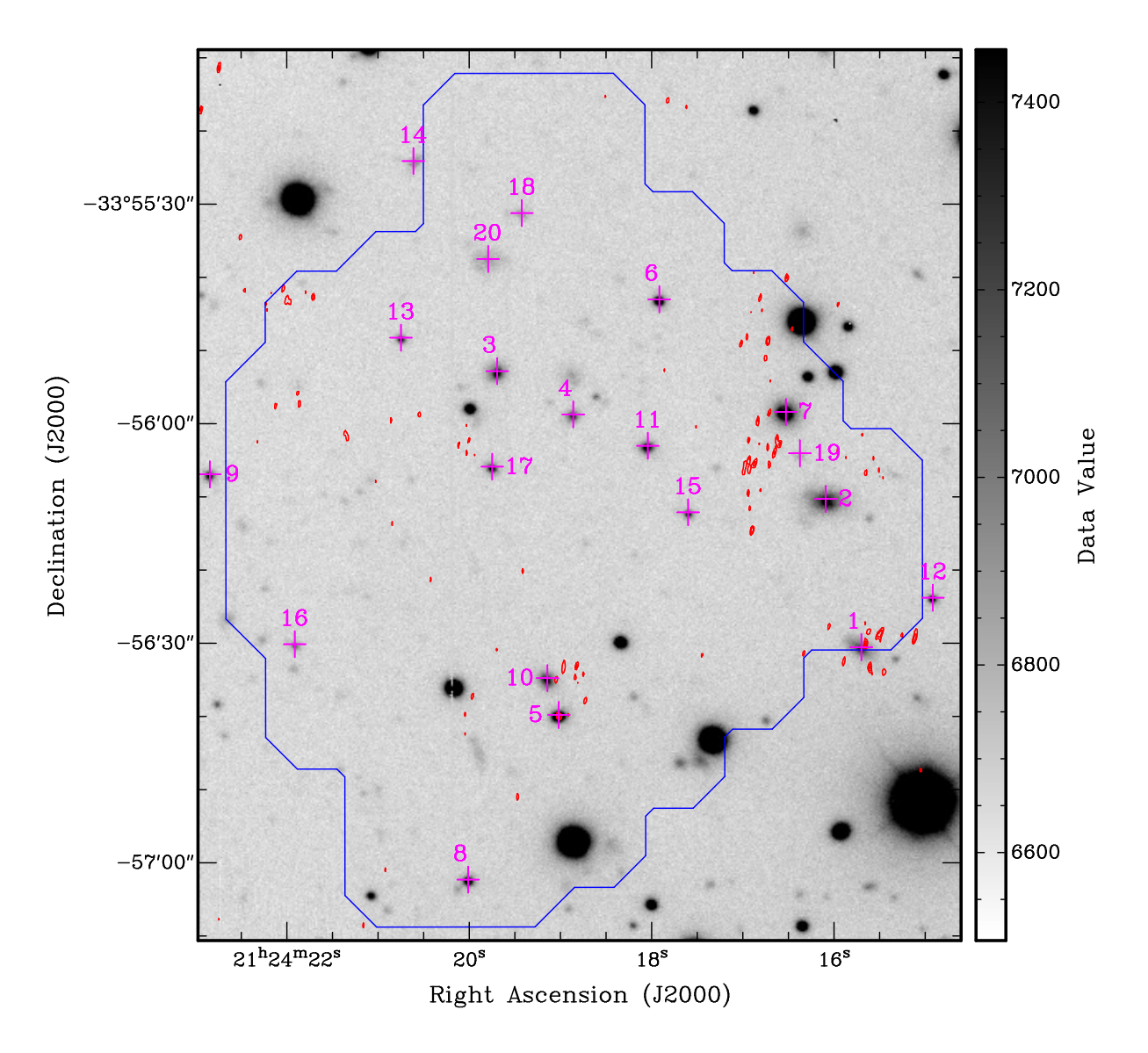


Figure 2. Overlay of radio contours from the VLA (red) on the greyscale GMOS r-band image. The contour levels are 3, 3.5, 4 times $5.7 \,\mu\text{Jy}$ beam⁻¹, which is the RMS noise of the off-source central regions of the image. The boundary of the localization region discussed in Section 4 is shown by a blue contour. The synthesized radio beam size of this image is quoted in Section 2. Magenta crosses and numbers represent the positions and source numbers of galaxies in Table 3. The length of the crosses is arbitrary and does not represent the positional uncertainty. Stellar objects in the localization region above our magnitude limits are reported in Table 3.

studied by Cheung (2007); Roberts et al. (2015); Saripalli & Roberts (2018); Roberts et al. (2018); Lal et al. (2019); Joshi et al. (2019). This appears to be an uncataloged example of such galaxies, as a cross-check of published lists of X-shaped sources Cheung (2007); Yang et al. (2019); Proctor (2011), did not include this object. While the object was detected as a 7.7 mJy beam $^{-1}$ radio source in the 1.4 GHz NVSS survey (Condon et al. 1998), the ${\sim}45''$ NVSS resolution caused the survey to detect this object as a point source.

6. DISCUSSION

6.1. Association Probability of Sources

We followed three approaches to calculate the probability of chance coincidence of the FRB with the sources in the error region. We followed two procedures described in Eftekhari & Berger (2017, Sec. 2 and 3) to calculate the probability without and with using the estimated redshift of the FRB. The first approach assumes a Poisson distribution of radio sources across the sky

Table 3. Optical sources detected within the localization region. Phot. Redshift is the photometric redshift of the source. VLA F_{peak} is the peak flux in the VLA radio image at the source location. Chance Assoc. Prob. (EB17) is the chance association probability of the source with FRB 180309.

Source	J2000		Photometric magnitudes (AB)			Phot.	VLA F_{peak}	Chance Assoc.	
No.	R.A.	Dec.	g	r	i	z	$Redshift^a$	$(\mu \text{Jy/beam})^b$	Prob. $(EB17)^{C}$
1	21:24:15.701	-33:56:30.55	22.36 ± 0.07	21.60 ± 0.04	20.46 ± 0.08	20.87 ± 0.05	$0.16^{+0.53}_{-0.07}$	24.28	0.99
2	21:24:16.090	-33:56:10.29	21.12 ± 0.06	20.47 ± 0.04	19.78 ± 0.08	19.61 ± 0.04	$0.31^{+0.41}_{-0.25}$	<19.5	0.76
3	21:24:19.693	-33:55:52.82	22.22 ± 0.06	21.60 ± 0.04	21.05 ± 0.08	21.03 ± 0.06	$0.42^{+0.26}_{-0.33}$	<16.8	0.99
4	21:24:18.860	-33:55:58.73	23.10 ± 0.07	22.43 ± 0.04	21.99 ± 0.09	_	$0.47^{+0.66}_{-0.43}$	<16.5	1.0
5	21:24:19.018	-33:56:39.80	22.00 ± 0.06	21.25 ± 0.04	20.46 ± 0.08	20.23 ± 0.03	$0.52^{+0.25}_{-0.44}$	22.1	0.96
6	21:24:17.916	-33:55:43.00	22.28 ± 0.06	21.81 ± 0.04	21.19 ± 0.08	21.09 ± 0.05	$0.53^{+0.24}_{-0.45}$	<17.1	1.0
7	21:24:16.529	-33:55:58.40	21.71 ± 0.06	20.38 ± 0.04	19.36 ± 0.07	19.20 ± 0.03	$0.55^{+0.11}_{-0.34}$	<19.2	0.73
8	21:24:20.012	-33:57:02.30	22.85 ± 0.07	21.93 ± 0.04	21.04 ± 0.08	20.93 ± 0.05	$0.56^{+0.17}_{-0.44}$	< 15.72	1.0
9	21:24:22.844	-33:56:06.92	22.56 ± 0.07	22.38 ± 0.04	22.19 ± 0.10	_	$0.62^{+0.64}_{-0.57}$	<15.93	1.0
10	21:24:19.142	-33:56:34.77	22.44 ± 0.07	21.71 ± 0.04	20.84 ± 0.08	20.85 ± 0.06	$0.65^{+0.09}_{-0.57}$	<17.7	0.99
11	21:24:18.042	-33:56:03.02	22.32 ± 0.06	21.98 ± 0.04	21.26 ± 0.08	21.54 ± 0.08	$0.66^{+0.09}_{-0.58}$	< 17.85	1.0
12	21:24:14.916	-33:56:23.78	23.80 ± 0.08	22.66 ± 0.04	21.58 ± 0.08	21.26 ± 0.06	$0.66^{+0.14}_{-0.15}$	<18.9	1.0
13	21:24:20.748	-33:55:48.25	24.12 ± 0.09	22.94 ± 0.04	21.37 ± 0.08	21.09 ± 0.05	$0.70^{+0.18}_{-0.09}$	<17.4	1.0
14	21:24:20.612	-33:55:24.12	23.97 ± 0.09	23.13 ± 0.05	22.43 ± 0.11	_	$0.71^{+0.70}_{-0.57}$	<18.0	1.0
15	21:24:17.600	-33:56:12.12	23.80 ± 0.08	22.80 ± 0.04	21.39 ± 0.08	20.98 ± 0.05	$0.76^{+0.17}_{-0.13}$	<18.6	1.0
16	21:24:21.913	-33:56:30.13	23.85 ± 0.08	23.38 ± 0.05	22.79 ± 0.11	_	$0.82^{+0.70}_{-0.67}$	<15.9	1.0
17	21:24:19.748	-33:56:05.88	22.43 ± 0.06	22.34 ± 0.04	21.32 ± 0.08	20.97 ± 0.06	$0.87^{+0.40}_{-0.12}$	<16.8	1.0
18	21:24:19.423	-33:55:31.22	23.43 ± 0.08	23.43 ± 0.06	23.04 ± 0.12	_	$0.99^{+0.61}_{-0.80}$	<17.7	1.0
19	21:24:16.375	-33:56:04.05	24.66 ± 0.11	24.27 ± 0.09	23.43 ± 0.14	_	$1.08^{+1.02}_{-0.57}$	<19.2	1.0
20	21:24:19.793	-33:55:37.49	22.46 ± 0.07	23.89 ± 0.09	21.13 ± 0.08	21.14 ± 0.06	$1.45^{+0.16}_{-0.10}$	<17.4	1.0

^aPhotometric redshifts correspond to the z_{peak} parameter from EAZY, and the uncertainties correspond to the 95% c.l. interval.

^c Probability was calculated using r-band magnitudes after correcting for extinction, $A_{\lambda} = 0.179$ (Schlafly & Finkbeiner 2011).

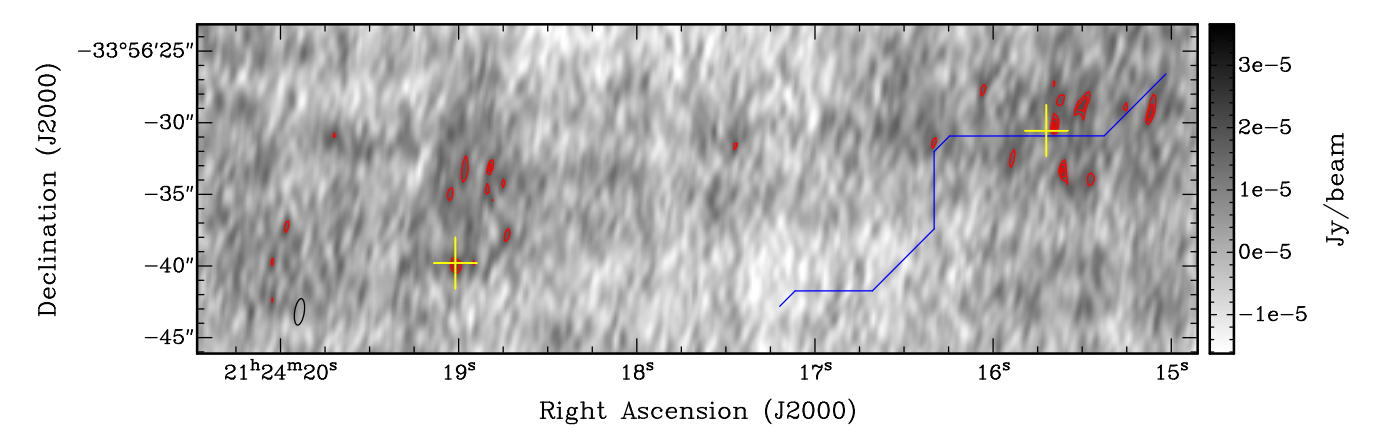


Figure 3. Sources within the localization region with a radio - optical overlap. The background grayscale and red contours are from VLA radio data. The boundary of the localization region is shown with a blue contour. The best fit optical position of the galaxies is shown with yellow crosses. The radio contours levels are placed at $5.7 \,\mu$ Jy beam⁻¹ times [3, 3.5, 4]. VLA beam is shown as a black ellipse in the bottom left.

^b For sources with intensity less than the local 3σ image RMS, we have reported the 3σ RMS. The intensities of source 1 and 5 are more than 3σ , but the signal-to-noise are low (< 6), so we have reported flux at the peak pixel.

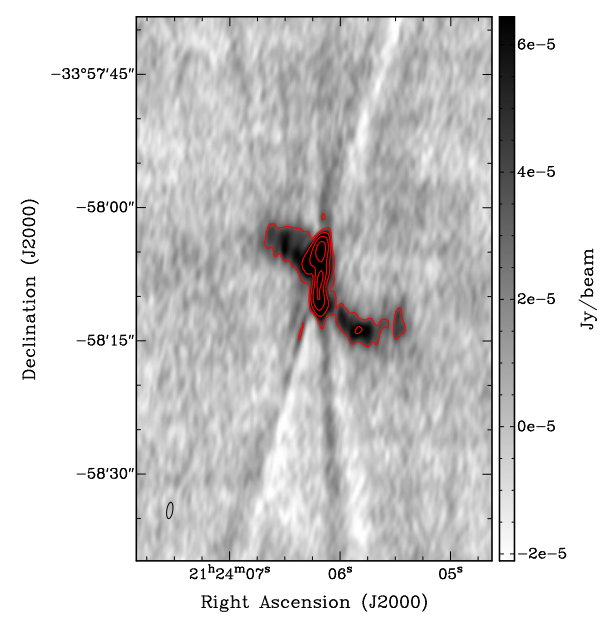


Figure 4. Radio image of the serendipitous (unrelated) source detection in our field. The background image and red contours are from VLA radio data. The radio contours levels are placed at $5.7 \,\mu\text{Jy} \,\text{beam}^{-1}$ times factors of [6, 12, 24, 48]. Note that the straight diagonal lines are due to side lobes and are an artifact of the imaging process.

and calculates the chance coincidence probability using the number density of galaxies above a limiting r-band magnitude. In the second approach, the number density of galaxies at a given redshift is calculated by integrating the optical luminosity functions. We also use the approach of Bloom et al. (2002, Sec. 6.1), which used the r band magnitude and the expression given by Hogg et al. (1997) to calculate the expected number of galaxies within a given radius. This is then used to calculate the corresponding association probability (Aggarwal 2021). Some details of the above methods are given in Appendix A.

We calculated the chance coincidence probability of all the sources given in Table 3, after correcting the r-band magnitudes for Galactic extinction (Schlafly & Finkbeiner 2011). We do not report the probabilities calculated using Bloom et al. (2002) and redshift approach of Eftekhari & Berger (2017) in Table 3, as they were all \sim 1. As no bright optical source was seen within the localization region, and because the localization region was large, the chance coincidence probability for all these associations were close to 1. Therefore, we cannot confidently associate FRB 180309 with any of the observed galaxies based on spatial coincidence information alone.

6.2. Plausible Host Galaxies

Here, we discuss the properties of the detected galaxies within the FRB error region and discuss the implications of their radio/optical properties.

6.2.1. Photometric Redshift Comparison

In Figure 5, we compare the galaxy photometric redshifts with the range of FRB redshifts previously estimated (z=0.13–0.32). While only two galaxies have most-likely photometric redshift values that lie within our estimated FRB redshift range, the photometric redshift errors are relatively large, thus do not preclude other galaxies from remaining contenders for the FRB host (in addition to dwarf galaxies below the detection limit of our observations, as we discuss in Section 6.2.4). However, five galaxies in this field (source numbers 12, 13, 15, 17, 19, 20 in Table 2) are unlikely hosts for the FRBs based on redshift information.

6.2.2. Using Coincident Radio/Optical Detections

Thus far, only one FRB—the repeating FRB 121102—has had a detection of any co-located "persistent" (non-bursting) radio emission. Other localized FRBs have reported strict limits on co-located emission, typically limits corresponding to a few tens of μ Jy (Bannister et al. 2019; Prochaska & Zheng 2019; Ravi et al. 2019; Marcote et al. 2020). Additionally, most progenitor models do predict, to some level, a radio counterpart (Platts et al. 2019). It is thus pertinent to search for any galaxies with associated radio emission in this region.

There were only two optical galaxies within the localization region that had a coincident borderline detection in the radio image. These were sources at photometric redshifts of $0.16^{+0.53}_{-0.07}$ ("source 1") and $0.52^{+0.25}_{-0.44}$ ("source 5"). Because the intensity of these sources is not sufficiently confident to perform reliable source fitting (signal-to-noise ratio <5), in Table 3 we report the flux at the peak pixel for each of the two radio components. The fluxes of these sources correspond to luminosities of $1.7 \times 10^{21} \, \mathrm{W \, Hz^{-1}}$ and $2.4 \times 10^{22} \, \mathrm{W \, Hz^{-1}}$ at their respective photometric redshifts. The luminosity of source 5 is comparable to that of the persistent radio source (PRS) of FRB 121102, while that of source 1 is an order of magnitude lower. We do not have a sufficiently strong detection to comment on the precise origin of this emission (star formation, AGN, or other).

The photometric redshifts of these sources are consistent with the redshift ranges we have estimated for FRB 180309. But, due to large errors on photometric redshifts, neither link is conclusive for the association. Further, as previously noted, these two radio sources may feasibly be arising due to diffuse, residual side-lobe

⁵ Implemented in https://github.com/KshitijAggarwal/casp

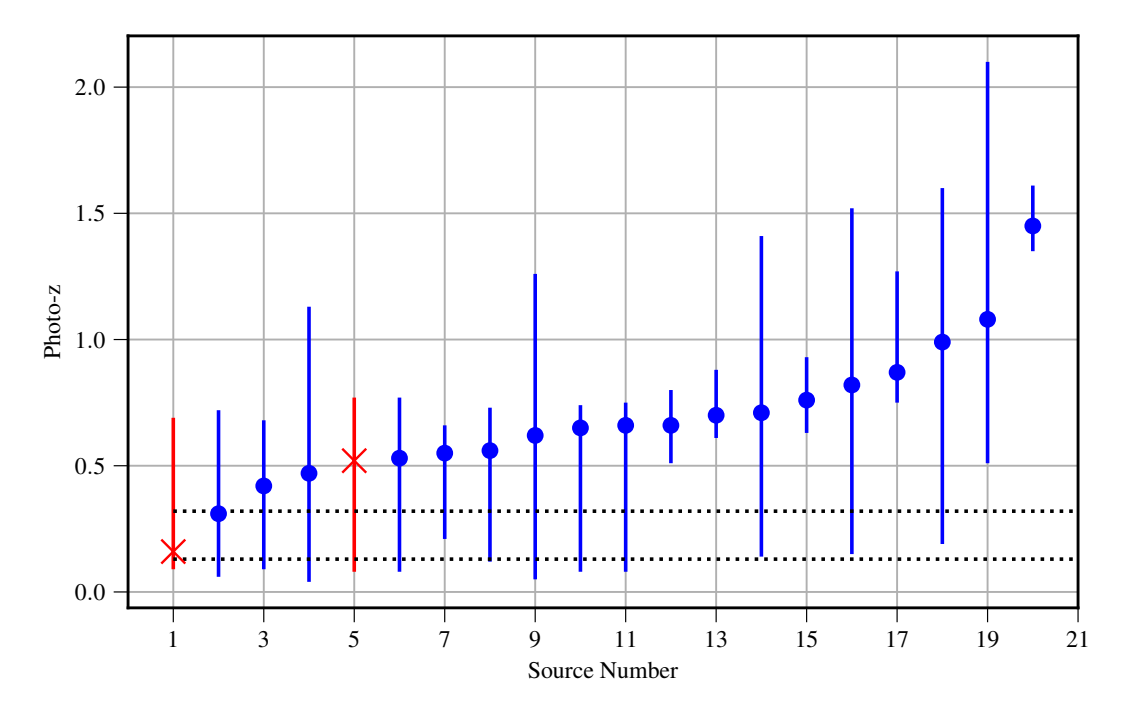


Figure 5. A comparison of the galaxy photometric redshifts with the FRB redshift estimated for two different formulations of the DM-redshift relation (Section 3). The blue points with errors represent all galaxies within the localization error region of FRB 180309, while the red crosses with errors represent the galaxies with a potential radio association also within the error region. The black dotted line shows the FRB redshift estimates. It is clear that while some galaxy associations can be ruled out, due to the large errors in our photometric redshift measurements, many galaxies in this sample remain host candidates based on redshift criteria.

structure in our radio image caused by low-level calibration errors and a bright foreground source at J2000 R.A.= $21^{\rm h}24^{\rm m}14^{\rm s}.749(2)$, Decl.= $-33^{\circ}47'58''.67(8)$.

6.2.3. Redshift-dependent Radio Luminosity Limit

The RMS limit of our VLA observations was $5.7\,\mu\mathrm{Jy\,beam^{-1}}$ in this field, which corresponds to a 3σ upper limit of $17.1\,\mu\mathrm{Jy\,beam^{-1}}$ on the flux of any persistent radio source. This, in turn, corresponds to luminosity limits of $<7.8\times10^{20}\,\mathrm{W\,Hz^{-1}}$ and $<5.8\times10^{21}\,\mathrm{W\,Hz^{-1}}$ at distances corresponding to redshifts of 0.13 and 0.32, respectively (the luminosity limit as a function of redshift is shown in Figure 6). The luminosity limits in this redshift range are lower than the luminosity of the PRS of FRB 121102 ($<1.93\times10^{22}\,\mathrm{W\,Hz^{-1}}$). Therefore, if FRB 180309 had a PRS similar to that of FRB 121102, then we could have detected it out to a redshift of 0.52 (see Fig 6).

So far, only FRB 121102 has been co-located with a PRS, with no other localized FRBs having a clearly identified radio counterpart. The redshift-dependent luminosity limits we show in Figure 6 are comparable to upper limits from other experiments that have not detected a PRS (Marcote et al. 2020; Macquart et al. 2020; Law et al. 2020; Ravi et al. 2019; Bannister et al. 2019; Prochaska & Zheng 2019). Given the variety of proper-

ties of FRB associations, it is possible that galaxies other than those with detectable radio emission in this field could feasibly remain the FRB 180309 host. In addition, as previously indicated, it remains possible that the PRS of FRB 121102 is unrelated to the FRB or its progenitor, therefore the presence of radio emission might not be specifically indicative of an FRB/host association.

6.2.4. Analysis of Whether We Detected All Likely Candidate Hosts

Using the magnitude limit of our optical observations, we can estimate the completeness for different galaxy types. Our r-band apparent magnitude limit of 24.3 translates to an absolute magnitude limit of -14.6 and -16.8 at the redshifts of 0.13 and 0.32, respectively.

Figure 7 shows the optical limit of our observations as a function of redshift. It also shows absolute magnitudes of host galaxies of localized FRBs with respect to their redshifts (Macquart et al. 2020; Bannister et al. 2019; Ravi et al. 2019; Bhandari et al. 2020; Law et al. 2020; Prochaska et al. 2019; Chatterjee et al. 2017; Heintz et al. 2020). The magnitude limits at these redshifts are higher than those of host galaxies of localized FRBs. Therefore, if the host galaxy of FRB 180309 is similar to that of other localized FRBs, then we would have de-

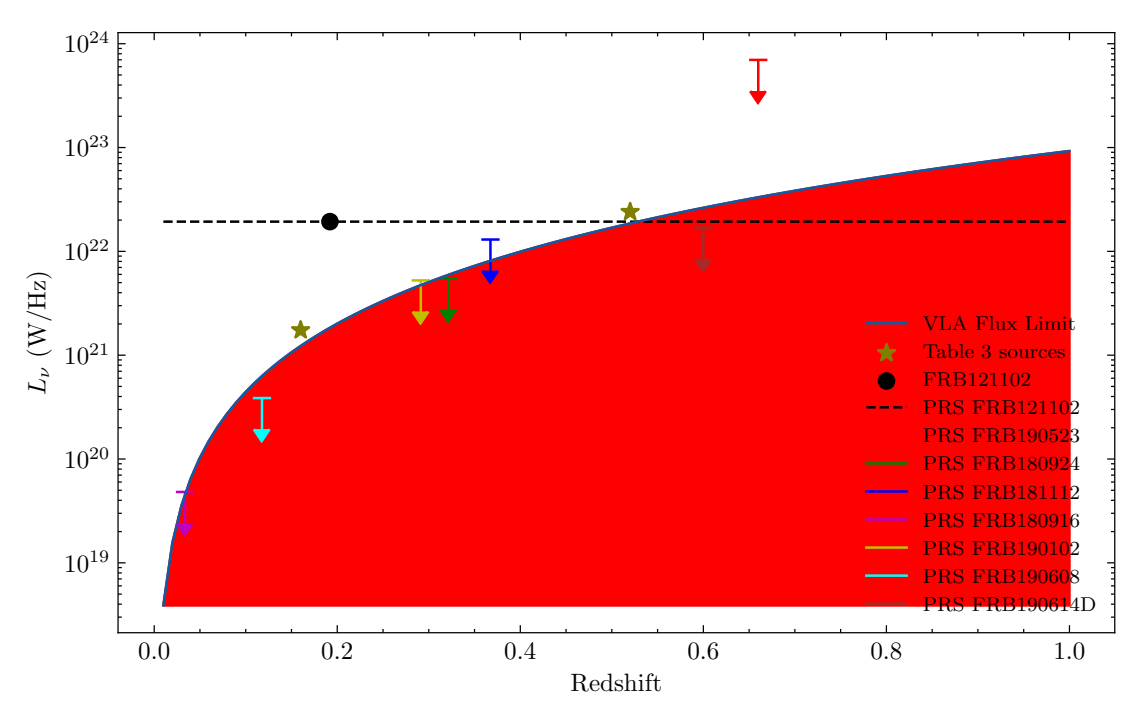


Figure 6. The blue solid line is the luminosity limit (corresponding to VLA flux limit of our observations) with respect to redshift. Black dashed line and point are the luminosity of PRS of FRB 121102. Upper limits on the luminosity of PRS corresponding to other localized FRBs are shown with downward pointing arrows. Olive stars correspond to the coincident sources discussed in Section 5.2. Note that due to large photo-z uncertainty, there is a considerable uncertainty in the luminosity of these coincident sources. Sources within the red shaded region would not be detected with our observations.

tected it: the host galaxy would be one of the galaxies in Table 3.

Our observations were also complete to all Milky Way type galaxies ($M \sim -21$) and all bright elliptical galaxies within the redshift upper limit for FRB 180309.

Thus, it seems likely that we have narrowed down the host to one of those listed in Table 3. However, a caveat to this analysis is that, as our observations were not complete to dwarf galaxies, we would not have detected the host galaxy of FRB 121102 (Fig 7). Similarly, we are also much less complete to low-surface brightness galaxies (Impey & Bothun 1997), but thus far, no FRB has been localized or associated to these galaxies.

6.3. Luminosity of the FRB

Osłowski et al. (2019) estimated the fluence of FRB 180309 to be $> 83.5\,\mathrm{Jy\,ms}$ (see their section 4.1 for details). This translates to a luminosity of $> 8.7\times10^{32}\,\mathrm{erg\,Hz^{-1}}$ at the redshift of 0.32 (the redshift upper limit for FRB 180309). We can compare this with the luminosities of all localized FRBs (Macquart et al. 2020; Marcote et al. 2020; Law et al. 2020; Bhandari et al. 2020; Bannister et al. 2019; Ravi et al. 2019; Prochaska et al. 2019; Chatterjee et al. 2017). Within this sample, we find that FRB 180309 is the second most luminous FRB (with one-sixth the luminosity of the most luminous localized FRB, FRB 190523). However, it may be

much brighter given we have only a lower limit on its fluence and an upper limit on the redshift. Moreover, it is likely that FRBs exhibit beamed emission which introduces an inherent uncertainty in comparing observed fluences.

7. CONCLUSION

We report the results of multi-wavelength follow-up observations of FRB 180309 to search for a host galaxy and non-bursting persistent radio emission. FRB 180309 was detected by Parkes Telescope during PPTA observations and is one of the brightest FRB detected with the Parkes Telescope to date. We used the multi-beam detection of this FRB to improve the localization precision to a $\sim 2' \times 2'$ region, a factor of ~ 37 improvement when compared with a typical localization with the Parkes Telescope. We estimated the redshift of this FRB to lie in the range 0.13–0.32. In our Gemini observations, we identified 20 galaxies within the localization error region. We found that the error region is still sufficiently large—and the galaxies' magnitudes sufficiently faintthat we could not confidently associate any of these sources with FRB 180309. Two of these galaxies also had a potential co-located VLA radio detection, however, these serve as only weak candidates for any persistent radio emission. No other coincident radio sources were found above the 3σ limit of 17.1μ Jy beam⁻¹. If

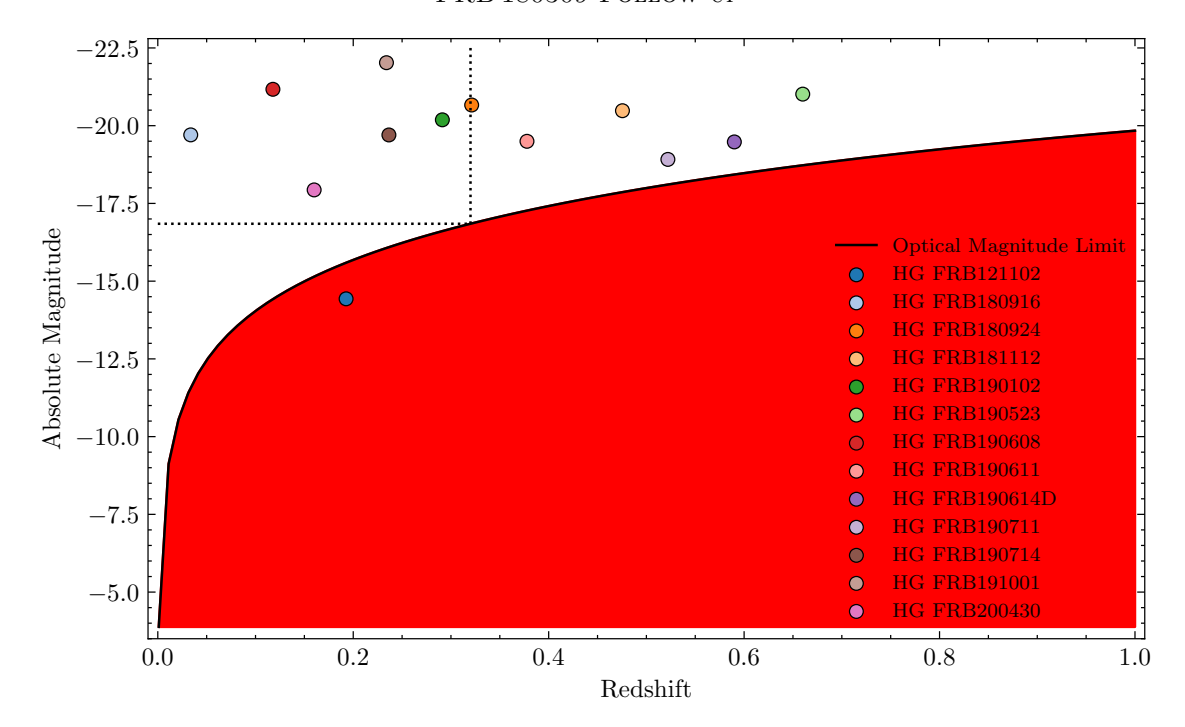


Figure 7. The black solid line is the optical absolute magnitude limit (corresponding to our Gemini r-band apparent magnitude limit of 24.3) with respect to redshift. Absolute magnitudes of host galaxies of localized FRBs are shown with colored circles. The black dotted line represents the absolute magnitude limit of our observations at the upper limit of redshift (z = 0.32) for FRB 180309. Sources within the red shaded region would not be detected with our observations.

a putative PRS of FRB 180309 were similar to that of FRB 121102, we would have detected it out to the farthest likely redshift of FRB 180309. We did not detect any time-varying or appropriately redshifted H I feature in our ATCA observations.

Far from our localization region, but within our radio imaging field, we detected a complex X-shaped source (J2124-3358). The morphology of this source is similar to the S-shaped sources reported in the literature.

Ultimately, a comparison of the photometric redshifts of our 20 candidate host galaxies with the DM-based redshift range of FRB 180309 resulted in 14 galaxies remaining as the most likely hosts of this FRB. While it is beyond the scope of this work, follow-up spectroscopy and in-depth analysis of the ionization content (i. e. potential for host DM contribution) for each of these galaxies may help reveal which galaxy is the host of this luminous FRB. Moreover, it might not be possible to unambiguously identify its host galaxy unless this FRB is detected to repeat and localized by an interferometer.

ACKNOWLEDGEMENTS

KA and SBS acknowledge support from NSF grant AAG-1714897. N.T. acknowledges support by FONDE-CYT grant 11191217. G.P acknowledges support by the Millennium Science Initiative ICN12_009. Based on observations obtained at the international Gemini Obser-

vatory, a program of NSF's OIR Lab, which is managed by the Association of Universities for Research in Astronomy (AURA) under a cooperative agreement with the National Science Foundation, on behalf of the Gemini Observatory partnership: the National Science Foundation (United States), National Research Council (Canada), Agencia Nacional de Investigación y Desarrollo (Chile), Ministerio de Ciencia, Tecnología e Innovación (Argentina), Ministério da Ciência, Tecnologia, Inovações e Comunicações (Brazil), and Korea Astronomy and Space Science Institute (Republic of Korea). The Gemini data was obtained from program GS-2018A-Q-205 and processed using the Gemini Pyraf package⁶ (Science Software Branch at STScI 2012). The National Radio Astronomy Observatory is a facility of the National Science Foundation operated under cooperative agreement by Associated Universities, Inc. The Common Astronomy Software Applications (CASA) package is software produced and maintained by NRAO. The Australia Telescope Compact Array (ATCA) is part of the Australia Telescope National Facility which is funded by the Australian Government for operation as a National Facility managed by CSIRO. We acknowledge the Gomeroi people as the traditional owners of the

⁶ https://www.gemini.edu/sciops/data-and-results/ processing-software/

ATCA site. The Parkes radio telescope is part of the Australia Telescope National Facility which is funded by the Australian Government for operation as a National Facility managed by CSIRO. We acknowledge the Wiradjuri people as the traditional owners of the Observatory site.

Facilities: EVLA, Gemini, ATCA

Software: astropy (Astropy Collaboration et al. 2013; Price-Whelan et al. 2018), karma (Gooch 1996), CASA (McMullin et al. 2007), numpy (Harris et al. 2020), matplotlib (Hunter 2007), pandas (pandas development team 2020)

APPENDIX

A. ASSOCIATION PROBABILITY CALCULATION

The chance association probability of an FRB to a host galaxy depends significantly on the surface density of the galaxies on the sky, offset of the source from the galaxy and localisation uncertainties. Following Bloom et al. (2002, hereafter B02) and Eftekhari & Berger (2017, hereafter EB17) we calculated the localization region (R) using $R = \max[2R_{FRB}, \sqrt{R_0^2 + 4R_h^2}]$, where R_{FRB} is the 1 σ localization radius of the FRB, R_0 is the radial angular separation between the FRB position and a presumed host, and R_h is the galaxy half-light radius. We use typical values of R_0 and R_h for LGRB and SLSN host galaxies, as given in EB17.

For the chance probability calculation, we followed Section 2 of EB17. We did a 3rd order spline fit to the r-band galaxy number counts given in Table 3 of Driver et al. (2016). In cases where multiple number counts were present corresponding to the same magnitude bin, we chose the one with the least cosmic variance. We did not weight our magnitude bins using cosmic variance for the spline fit. The probability of chance coincidence was then defined as in equation 1 of EB17.

Further, we also followed Section 3 of EB17, to use the redshift constraint on the FRB to estimate the chance association probability. Here, relationships between DM and z are used to estimate the likely range in redshift of the FRB from its DM (Macquart et al. 2020; Pol et al. 2019; Ioka 2003; Inoue 2004). We calculate the number density of galaxies by integrating optical luminosity functions presented in Beare et al. (2015, Table 6, blue galaxies) for 0.2 < z < 1.2 and Blanton et al. (2003) for z < 0.1. To estimate the luminosity function for 0.1 < z < 0.2, we averaged the luminosity function parameters for z < 0.1 and 0.2 < z < 0.4 (T. Eftekhari private communication). The chance association probability is then given by:

$$P_{cc} = 1 - e^{-f_A N(\leq M, \leq z)} \tag{A1}$$

Here, $f_A = \pi R^2/5.346 \times 10^{11}$ is the fractional area of the localization region on the sky, where R is in arcseconds. $N(\leq M, \leq z)$ is the total number of galaxies above a limiting absolute magnitude M, within a comoving volume out to a redshift z. As luminosity functions are different for different redshift bins, we calculated the number of galaxies in each redshift bin individually. The number of galaxies in each bin is calculated by integrating the luminosity functions from absolute magnitude of -24 to absolute magnitude corresponding to $0.01L^*$ galaxy, multiplied by the comoving volume of that redshift annuli. The total number of galaxies was obtained by adding the number of galaxies from the lowest redshift bin (i.e. 0 < z < 0.1) to that including max redshift (z_{max}) bin.

We also provide casp⁷: Calculating ASsociation Probability of FRBs, which is a python package (Aggarwal 2021) and a webpage⁸ to calculate association probability of FRBs using B02; EB17.

REFERENCES

Aggarwal, K. 2021, KshitijAggarwal/casp: 0.1.0, 0.1.0,
Zenodo, doi: 10.5281/zenodo.4543665
Astropy Collaboration, Robitaille, T. P., Tollerud, E. J.,
et al. 2013, A&A, 558, A33,
doi: 10.1051/0004-6361/201322068

Bannister, K. W., Deller, A. T., Phillips, C., et al. 2019,Science, doi: 10.1126/science.aaw5903Bassa, C. G., Tendulkar, S. P., Adams, E. A. K., et al.

2017, ApJL, 843, L8, doi: 10.3847/2041-8213/aa7a0c

Beare, R., Brown, M. J. I., Pimbblet, K., Bian, F., & Lin, Y.-T. 2015, ApJ, 815, 94,

doi: 10.1088/0004-637X/815/2/94

⁷ https://github.com/KshitijAggarwal/casp

⁸ https://kshitijaggarwal.github.io/casp/

- Bertin, E., & Arnouts, S. 1996, A&AS, 117, 393, doi: 10.1051/aas:1996164
- Bhandari, S., Sadler, E. M., Prochaska, J. X., et al. 2020, ApJL, 895, L37, doi: 10.3847/2041-8213/ab672e
- Blanton, M. R., Hogg, D. W., Bahcall, N. A., et al. 2003, ApJ, 592, 819, doi: 10.1086/375776
- Bloom, J. S., Kulkarni, S. R., & Djorgovski, S. G. 2002, AJ, 123, 1111, doi: 10.1086/338893
- Bochenek, C. D., Ravi, V., Belov, K. V., et al. 2020, Nature, 587, 59, doi: 10.1038/s41586-020-2872-x
- Brammer, G. B., van Dokkum, P. G., & Coppi, P. 2008, ApJ, 686, 1503, doi: 10.1086/591786
- Burke-Spolaor, S., Bailes, M., Ekers, R., Macquart, J.-P., & Crawford, III, F. 2011, ApJ, 727, 18, doi: 10.1088/0004-637X/727/1/18
- Chatterjee, S., Law, C. J., Wharton, R. S., et al. 2017, Nature, 541, 58, doi: 10.1038/nature20797
- Cheung, C. C. 2007, AJ, 133, 2097, doi: 10.1086/513095
- CHIME/FRB Collaboration, Andersen, B. C., Bandura, K. M., et al. 2020, Nature, 587, 54, doi: 10.1038/s41586-020-2863-y
- Condon, J. J., Cotton, W. D., Greisen, E. W., et al. 1998, AJ, 115, 1693, doi: 10.1086/300337
- Cordes, J. M., & Lazio, T. J. W. 2002, arXiv Astrophysics e-prints
- Driver, S. P., Andrews, S. K., Davies, L. J., et al. 2016, ApJ, 827, 108, doi: 10.3847/0004-637X/827/2/108
- Eftekhari, T., & Berger, E. 2017, ApJ, 849, 162, doi: 10.3847/1538-4357/aa90b9
- Gimeno, G., Boucher, L., Chiboucas, K., et al. 2016, in American Astronomical Society Meeting Abstracts, Vol. 227, American Astronomical Society Meeting Abstracts #227, 445.01
- Gooch, R. 1996, Astronomical Society of the Pacific Conference Series, Vol. 101, Karma: a Visualization Test-Bed, ed. G. H. Jacoby & J. Barnes, 80
- Harris, C. R., Millman, K. J., van der Walt, S. J., et al. 2020, Nature, 585, 357, doi: 10.1038/s41586-020-2649-2
- Heintz, K. E., Prochaska, J. X., Simha, S., et al. 2020, ApJ, 903, 152, doi: 10.3847/1538-4357/abb6fb
- Hogg, D. W., Pahre, M. A., McCarthy, J. K., et al. 1997, MNRAS, 288, 404, doi: 10.1093/mnras/288.2.404
- Hook, I. M., Jørgensen, I., Allington-Smith, J. R., et al. 2004, PASP, 116, 425, doi: 10.1086/383624
- Hunter, J. D. 2007, Computing in Science & Engineering, 9, 90, doi: 10.1109/MCSE.2007.55
- Impey, C., & Bothun, G. 1997, ARA&A, 35, 267, doi: 10.1146/annurev.astro.35.1.267
- Inoue, S. 2004, MNRAS, 348, 999, doi: 10.1111/j.1365-2966.2004.07359.x

- Ioka, K. 2003, ApJL, 598, L79, doi: 10.1086/380598Joshi, R., Krishna, G., Yang, X., et al. 2019, ApJ, 887, 266,
- doi: 10.3847/1538-4357/ab536f
- Kirsten, F., Snelders, M. P., Jenkins, M., et al. 2020, Nature Astronomy, doi: 10.1038/s41550-020-01246-3
- Kron, R. G. 1980, ApJS, 43, 305, doi: 10.1086/190669
- Lal, D. V., Sebastian, B., Cheung, C. C., & Rao, A. P. 2019, The Astronomical Journal, 157, 195, doi: 10.3847/1538-3881/ab1419
- Law, C. J., Butler, B. J., Prochaska, J. X., et al. 2020, ApJ, 899, 161, doi: 10.3847/1538-4357/aba4ac
- Lorimer, D. R., Bailes, M., McLaughlin, M. A., Narkevic,
 D. J., & Crawford, F. 2007, Science, 318, 777,
 doi: 10.1126/science.1147532
- Macquart, J. P., Prochaska, J. X., McQuinn, M., et al. 2020, Nature, 581, 391, doi: 10.1038/s41586-020-2300-2
- Marcote, B., Paragi, Z., Hessels, J. W. T., et al. 2017, ApJL, 834, L8, doi: 10.3847/2041-8213/834/2/L8
- Marcote, B., Nimmo, K., Hessels, J. W. T., et al. 2020, Nature, 577, 190, doi: 10.1038/s41586-019-1866-z
- McMullin, J. P., Waters, B., Schiebel, D., Young, W., & Golap, K. 2007, Astronomical Society of the Pacific
 Conference Series, Vol. 376, CASA Architecture and
 Applications, ed. R. A. Shaw, F. Hill, & D. J. Bell, 127
- Osłowski, S., Shannon, R. M., Ravi, V., et al. 2019, MNRAS, 488, 868, doi: 10.1093/mnras/stz1751
- pandas development team, T. 2020, pandas-dev/pandas: Pandas 1.0.3, v1.0.3, Zenodo, doi: 10.5281/zenodo.3715232
- Petroff, E., Barr, E. D., Jameson, A., et al. 2016, PASA, 33, e045, doi: 10.1017/pasa.2016.35
- Planck Collaboration, Ade, P. A. R., Aghanim, N., et al. 2016, A&A, 594, A13, doi: 10.1051/0004-6361/201525830
- Platts, E., Weltman, A., Walters, A., et al. 2019, PhR, 821,1, doi: 10.1016/j.physrep.2019.06.003
- Pol, N., Lam, M. T., McLaughlin, M. A., Lazio, T. J. W.,
 & Cordes, J. M. 2019, ApJ, 886, 135,
 doi: 10.3847/1538-4357/ab4c2f
- Price-Whelan, A. M., Sipőcz, B. M., Günther, H. M., et al. 2018, AJ, 156, 123, doi: 10.3847/1538-3881/aabc4f
- Prochaska, J. X., Simha, S., Law, C., Tejos, N., & mneeleman. 2019, FRBs/FRB: First DOI release of this repository, v1.0.0, Zenodo, doi: 10.5281/zenodo.3403651
- Prochaska, J. X., & Zheng, Y. 2019, MNRAS, 485, 648, doi: 10.1093/mnras/stz261
- Prochaska, J. X., Macquart, J.-P., McQuinn, M., et al. 2019, Science, 366, 231, doi: 10.1126/science.aay0073
- Proctor, D. D. 2011, VizieR Online Data Catalog, 219

Rajwade, K. M., Pingel, N. M., Black, R. A., et al. 2018, inPulsar Astrophysics the Next Fifty Years, ed.P. Weltevrede, B. B. P. Perera, L. L. Preston, &

S. Sanidas, Vol. 337, 398–399,doi: 10.1017/S1743921317009012

- Ravi, V. 2019, MNRAS, 482, 1966, doi: 10.1093/mnras/sty1551
- Ravi, V., Shannon, R. M., Bailes, M., et al. 2016, Science, 354, 1249, doi: 10.1126/science.aaf6807
- Ravi, V., Catha, M., Addario, L. D., et al. 2019, Nature, doi: 10.1038/s41586-019-1389-7
- Roberts, D. H., Cohen, J. P., Lu, J., Saripalli, L., & Subrahmanyan, R. 2015, ApJS, 220, 7, doi: 10.1088/0067-0049/220/1/7
- Roberts, D. H., Saripalli, L., Wang, K. X., et al. 2018, ApJ, 852, 47, doi: 10.3847/1538-4357/aa9c49
- Saripalli, L., & Roberts, D. H. 2018, ApJ, 852, 48, doi: 10.3847/1538-4357/aa9c4b

- Sault, R. J., Teuben, P. J., & Wright, M. C. H. 1995, in Astronomical Society of the Pacific Conference Series,
 Vol. 77, Astronomical Data Analysis Software and
 Systems IV, ed. R. A. Shaw, H. E. Payne, & J. J. E. Haves, 433
- Schlafly, E. F., & Finkbeiner, D. P. 2011, ApJ, 737, 103, doi: 10.1088/0004-637X/737/2/103
- Science Software Branch at STScI. 2012, PyRAF: Python alternative for IRAF. http://ascl.net/1207.011
- Staveley-Smith, L., Wilson, W. E., Bird, T. S., et al. 1996, PASA, 13, 243
- Tendulkar, S. P., Bassa, C. G., Cordes, J. M., et al. 2017, ApJ Letters, 834, L7, doi: 10.3847/2041-8213/834/2/L7
- Tendulkar, S. P., Gil de Paz, A., Kirichenko, A. Y., et al. 2021, ApJL, 908, L12, doi: 10.3847/2041-8213/abdb38
- Ungruhe, R., Seitter, W. C., & Duerbeck, H. W. 2003, Journal of Astronomical Data, 9, 1
- Yang, X., Joshi, R., Gopal-Krishna, et al. 2019, ApJS, 245, 17, doi: 10.3847/1538-4365/ab4811
- Yao, J. M., Manchester, R. N., & Wang, N. 2017, ApJ, 835, 29, doi: 10.3847/1538-4357/835/1/29